

Chapter 2

Detectors for Small-Animal SPECT I

Overview of Technologies

Harrison H. Barrett and William C. J. Hunter*

barrett@radiology.arizona.edu

1. Introduction

Indirect imaging systems such as SPECT have three essential components: an image-forming element, an image detector, and a reconstruction algorithm. These components act together to transfer information about the object to the end user or *observer*, which can be a human or a computer algorithm. As we shall see in Chapter 5, the efficacy of this information transfer can be quantified and used as a figure or merit for the overall imaging system or for any component of it. Fundamentally, image quality is defined by the ability of some observer to perform some task of medical or scientific interest.

In many cases, the limiting factor in task performance is the image detector. Only when the detector is capable of recording finer spatial or temporal detail can more information be transferred to the observer. Conversely, any improvement in detector capability can be translated into improved task performance by careful design of the image-forming element and the reconstruction algorithm.

In the case of nuclear medicine with single-photon isotopes, however, it has long been the conventional wisdom that there is no need for improved detectors because the limiting factor is always the image-forming element. This view stems from consideration of the usual imaging configuration in which a parallel-bore collimator is placed in front of an image detector such as an Anger camera. To a reasonable approximation, the resolutions of the detector and collimator add in quadrature and, when the detector resolution is much better than that of the collimator, the latter dominates. Continuing the argument, many authors conclude that improvements in collimator resolution are obtainable only at the expense of photon-collection efficiency; thus there is little hope of any improvement in single-photon gamma-ray imaging.

*The University of Arizona, Department of Radiology, Tucson, Arizona

This chapter has two goals. The first is to show that the conventional wisdom is wrong, that improvements in detector capability can indeed be translated to measurable benefits in system performance in SPECT. The second goal is to survey the available technologies for improving detector performance, especially for small-animal applications.

Because detector requirements depend on the image-forming element, we begin in Section 2 by looking broadly at methods of image formation in gamma-ray emission imaging. As we shall see, pinhole imaging is an attractive alternative to parallel-hole collimators, with some perhaps unexpected advantages. In Section 3, we look more specifically at small-animal SPECT and assess the requirements on the gamma-ray detectors to be used there.

In Section 4, we examine the various physical mechanisms that might be used for gamma-ray detection. The unsurprising conclusion will be that semiconductor and scintillation detectors in various forms are the most promising; these two technologies will be examined in more detail in Sections 5 and 6, respectively.

2. Image formation

This section is a catalog of methods of forming images of emissive gamma-ray sources, with a few comments on applicability to small-animal SPECT. The reader is presumed to be familiar with the elementary properties of collimators and pinholes, but a review can be found in Barrett and Swindell [1981, 1996b].

2.1 Multi-bore collimators

Parallel-hole collimators made of lead are the image-forming elements of choice in clinical SPECT. Typically, for that application, the bore length is 2–3 cm, the bore diameter is 1–3 mm, and the septal thickness is of order 1 mm. These parameters are chosen to give a collimator resolution of 1 cm or so at a distance of about 15 cm from the collimator face. The resulting collimator efficiency (fraction of the emitted photons passed by the collimator) is around 3×10^{-4} .

Parallel-hole collimators also can be used for small-animal SPECT, but quite different parameters are needed. At the Center for Gamma-ray Imaging (CGRI), we use a laminated tungsten collimator with 7 mm bore length, 260 μm square bores, and 120 μm septa, yielding an efficiency of 5×10^{-5} and submillimeter resolution out to about 2.5 cm from the collimator face. Further improvement could be achieved by fabricating the collimator from gold, which is economically feasible for small animals but not for clinical applications.

Focusing collimators with nonparallel bores are sometimes used clinically to magnify or minify the object onto the camera face, but to the authors' knowledge, they have not been used for small animals.

For a thorough discussion of collimator design and optimization, see Gunter [1996].

2.2 Pinholes

2.2.1 Simple pinhole imaging. Most small-animal SPECT imaging today is done with pinholes. Pinholes are very flexible, with the main free parameters being the pinhole diameter d_{ph} , the perpendicular distance s_1 from the pinhole plane to an object plane of interest, and the perpendicular distance s_2 from the pinhole to the detector plane. The collection efficiency is controlled by the ratio $[d_{ph}/s_1]^2$, while the magnification is given by s_2/s_1 . The spatial resolution depends on all three parameters and on the spatial resolution of the detector. As a general rule, the magnification should be adjusted so that the contribution of the detector to the overall spatial resolution is equal to or less than the contribution of the pinhole; with low-resolution detectors, a large magnification is very useful.

Other design considerations in pinhole imaging concern penetration of the radiation through the edges of the pinhole and vignetting in the imaging of off-axis points. For good discussions of these points, see Jaszczak et al. [1993] and Smith and Jaszczak [1998].

2.2.2 Multiple pinholes and coded apertures. With pinholes or collimators and a fixed imaging geometry, there is an inevitable tradeoff between photon-collection efficiency and spatial resolution; a smaller pinhole or collimator bore improves resolution but degrades efficiency. In practice, however, there is no reason for the imaging geometry to remain fixed. A simple way of avoiding the tradeoff in pinhole imaging is to use more pinholes; a system with N pinholes has N times the collection efficiency of a single pinhole of the same size. As long as the pinhole images do not overlap on the detector surface, the overall gain in sensitivity is also a factor of N .

As N increases, however, overlapping, or *multiplexing*, of the pinhole images occurs, and we refer to the multiple-pinhole system as a *coded aperture*. In that case, the system performance is no longer simply related to the collection efficiency. While it is true that the total number of detected photons increases by a factor of N , each photon conveys less information about the object because of the uncertainty about which pinhole it came through.

The effect of multiplexing on the noise properties of the images has been studied thoroughly for nontomographic imaging of planar objects; see Barrett and Swindell [1981, 1996b] for a discussion in terms of signal-to-noise ratio in the image and Myers et al. [1990] for a treatment in terms of detection tasks. In brief, for an object of finite size, the system performance increases linearly with N until the images overlap, after which the rate of improvement drops.

For tomographic (SPECT) imaging, it is important to realize that multiplexing *always* occurs, even for a single pinhole. One pinhole and one detector element define a tube-like region or *ray* through a 3D object, and emissions from all points along the ray contribute to the photon noise in that one detector reading. For detection of a nonrandom lesion in a uniform object, the effective degree of multiplexing for a single pinhole is of order L/δ , where L is the average length of the intersection of the ray with the object, and δ is the size of the lesion. If there are N pinholes, and

M rays through the object strike one detector element, the degree of multiplexing increases to ML/δ . Because the total number of counts is proportional to N , the detectability scales as $N\delta/ML$ (i.e., N divided by the degree of multiplexing). If there is no overlap of the pinhole images, then $M = 1$, and we gain the full benefit of N pinholes, just as in the planar case, but there is the additional loss of detectability (by a factor of δ/L) in any tomographic system due to multiplexing along the ray.

The degree of multiplexing is not the whole story, however, because performance on a task of clinical interest might be limited by object nonuniformity (anatomical noise) as well as by photon noise. As discussed more fully in Barrett and Myers [2004] and in Chapter 5 of this volume, the performance limitations arising from anatomical noise are related to the deterministic properties of the system rather than the stochastic properties such as Poisson noise. Discrimination against anatomical noise is best accomplished if the system collects sufficient data that an artifact-free reconstruction can be formed.

Early work in coded-aperture imaging did not satisfy this condition because projections were collected over a relatively small range of angles. As with any limited-angle tomography system, there were significant null functions which resulted in artifacts and loss of task performance in the presence of anatomical noise. More recent work has recognized that multiplexing and limited-angle imaging are two different problems, the main connection being that they both lead to null functions.

An example of a small-animal SPECT system that separates these two problems is the work of Schramm and co-workers at Jülich [Schramm et al., 2002]. In their work, a multiple-pinhole aperture is rotated around an animal so that a full range of view angles is sampled; excellent images are obtained despite multiplexing.

Meikle et al. [2002, 2003] are also developing coded-aperture systems for small-animal applications, using both multiple-pinhole apertures and Fresnel zone plates [Barrett, 1972]. By using up to four detector heads, the limited-angle problems are avoided, and generally artifact-free image are obtained in simulation.

Another recent project applying coded apertures to small-animal SPECT is the work at MIT using uniformly redundant arrays [Accorsi, 2001a, 2001b]. Originally developed for x-ray and gamma-ray astronomy, these arrays produce images that can be decoded to yield a sharp point spread function for an object that consists of a single plane. For 3D objects, they provide a form of longitudinal tomography or laminography in which one plane is in focus while other planes are blurred in some way, but the location of the in-focus plane can be varied in the reconstruction step. Promising results have been obtained despite the limited-angle nature of the data.

2.2.3 Pinholes and high-resolution detectors. A little-recognized aspect of multiple-pinhole imaging is that it allows us to gain sensitivity without sacrificing final image resolution, provided we can improve the detector performance. If we develop a detector with improved resolution, we can use it with a smaller pinhole or finer collimator and improve the final image resolution at the expense of sensitivity, but we can also use it to improve sensitivity. To do so, we move the detector closer to the pinhole, thereby reducing the magnification and leaving room for more pinholes

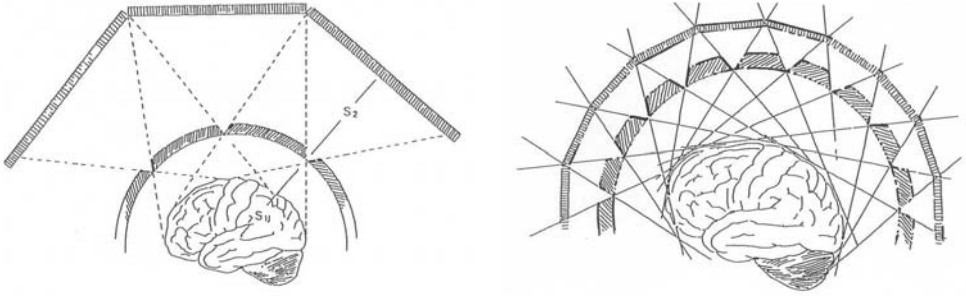


Figure 2.1. (Left) Illustration of a multi-pinhole imager used with low-resolution detectors. (Right) Illustration of a multi-pinhole used with high-resolution detectors. With the same final resolution and field of view as in the Left figure, the system illustrated to the Right can have much higher sensitivity.

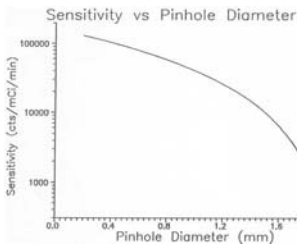


Figure 2.2. Sensitivity of an optimally designed system vs. pinhole diameter.

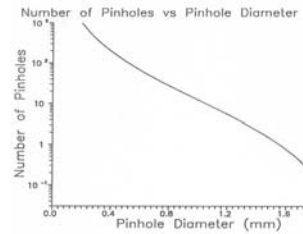


Figure 2.3. Allowed number of pinholes for no image overlap.

without encountering problems from overlapping or multiplexed images (see Fig. 2.1). Even though smaller pinholes are then needed for the same final resolution, the number of pinholes increases faster than the area of each decreases; thus, the overall sensitivity is actually increased [Rogulski, 1993]. The effect can be seen quantitatively in Figs. 2.2–2.4, taken from the Rogulski paper for the case of clinical brain imaging. Fig. 2.2 shows the paradoxical end result: the photon-collection efficiency *increases* as *smaller* pinholes are used. The explanation of the paradox is shown in Fig. 2.3; because the smaller pinholes are used with lower magnification, many more of them can be placed around the brain. The technological price one has to pay is shown in Fig. 2.4; the detector resolution must be much greater with the smaller pinholes and lower magnification if the same final resolution is to be maintained. Turning the argument around, if one has a certain detector resolution, Fig. 2.4 can be used to select a pinhole size which, with optimal choice of magnification, will lead to the specified resolution (2 mm for the graphs shown). Then Fig. 2.3 shows the number of pinholes that can be used without multiplexing, and Fig. 2.2 shows the resultant sensitivity.

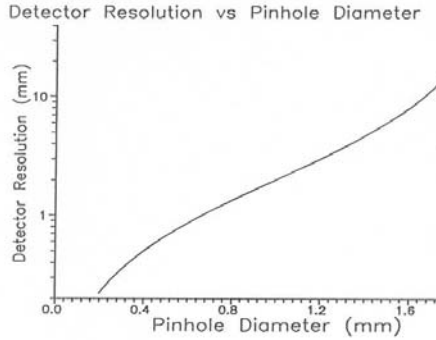


Figure 2.4. Required detector resolution in order to use a given pinhole diameter and the number of pinholes shown in Fig. 2.3 with constant final resolution (2 mm).

2.3 Synthetic collimators

There is still another way of using multiple pinholes, in a system that can be regarded as a hybrid between coded apertures and unmultiplexed pinholes. Referred to in our group as the *synthetic collimator*, this approach is designed to overcome the limitations of real collimators [Clarkson, 1999; Wilson, 2000].

To understand the objective of the synthetic collimator, let us first define an ideal parallel-hole collimator. This physically unrealizable device would acquire a two-dimensional (2D) projection of a 3D object with a spatial resolution and sensitivity independent of position in the object. More precisely, a detector element placed behind one bore of the ideal collimator would be uniformly sensitive to radiation emanating from anywhere in a tube-like region of space formed by mathematically extending the bore into the object, and it would be totally insensitive to radiation originating outside this tube. This detector would therefore measure the integral of the object activity over this tube region, and other detector elements would do the same for other tubes. The collection of tube integrals is the ideal planar projection. In a synthetic collimator, we attempt to collect a data set from which these tube integrals can be estimated by mathematical operations on actual data.

A suitable data set for this purpose can be collected by a simple multiple-pinhole aperture. A plate of gamma-ray-absorbing material is placed in the plane $z = 0$, and the object is contained in the halfspace $z > 0$. The plate is essentially opaque except for K small pinholes, and the image detector is placed in the plane $z = -s$. In the absence of noise, the m th detector element records a measurement given by

$$g_m = \int_S d^3\mathbf{r} f(\mathbf{r}) h_m(\mathbf{r}). \quad (2.1)$$

where \mathbf{r} is a 3D vector, $f(\mathbf{r})$ is the object activity, S is the region of support of the object, and $h_m(\mathbf{r})$ is the sensitivity function that specifies the response of the detector to radiation emanating from point \mathbf{r} . If the detector can "see" the object

through all K pinholes, then $h_m(\mathbf{r})$ is appreciable over K cone-like regions through the object.

The parameters we would like to estimate are the ideal tube integrals, given by

$$\theta_j = \int_S d^3\mathbf{r} f(\mathbf{r}) t_j(\mathbf{r}). \quad (2.2)$$

where $t_j(\mathbf{r})$ is the tube function, defined to be unity in the region of the j th tube and zero elsewhere. The key question is whether we can recover the values of θ_j from the measured data, at least in the absence of noise. The answer is yes if we can write the tube functions themselves as a linear superposition of the sensitivity functions, so that

$$t_j(\mathbf{r}) = \sum_{m=1}^M B_{jm} h_m(\mathbf{r}). \quad (2.3)$$

If this condition can be satisfied, then we can find all of the tube integrals by

$$\theta_j = \sum_{m=1}^M B_{jm} g_m. \quad (2.4)$$

When noise is taken into account, it is advantageous to estimate the tube integrals by maximum-likelihood (ML) methods such as the expectation-maximization (EM) algorithm, but the success of the synthesis still depends on being able to represent the tube functions as a linear superposition of sensitivity functions as in equation 2.3.

We have performed a large number of simulation studies to determine the circumstances under which this synthesis can be performed. In brief, we find that a single multiple-pinhole image is not sufficient. It is necessary to collect additional information, for example by varying the aperture-to-detector distance s , possibly with different pinhole patterns at each s . When we do this, the simulations and theoretical analysis show that an excellent approximation to the ideal collimator can be synthesized and that the results are quite robust to noise.

There are several ways to implement the synthetic-collimator concept in practice. One is to fix a multiple-pinhole plate relative to the object and to take data with several (3–4) spacings between the plate and the detector. The synthesis then gives a single 2D projection of the 3D object, and the object or the pinhole-detector assembly can be rotated to obtain multiple projections for 3D reconstruction. Alternatively, the data acquired with multiple detector distances but no rotation can be processed by ML methods to yield 3D images directly; the results with this approach are surprisingly good in practice, even though it is limited-angle tomography. A third approach combines the first two, acquiring data with 3 or 4 detector spacings and a few rotations, for example rotating the object in 45° steps. Finally, the requirement for mechanically moving the detector relative to the pinhole plate can be avoided by using several (say four) separate detectors, each with its own spacing s , and again rotating the object or the detector assembly to gather sufficient data for 3D reconstruction.

2.4 Other methods of image formation

At 140 keV, pinholes or collimators appear to be the only viable option for forming gamma-ray images. Approaches based on grazing-incidence reflective optics are of interest at much lower energies; they deserve attention for small-animal imaging, especially below 30 keV, but the grazing angles are quite small and probably impractical at higher energies. Similarly, multilayer thin films operated near normal incidence show promise at low energies but have very low efficiency at 30 keV and above. Approaches based on diffraction from crystals have shown good efficiency at high energies, but the requirement for matching the Bragg condition leads to systems with very long focal lengths and/or small fields of view.

At higher energies, an interesting approach to image formation in nuclear medicine is the Compton camera. In this method, there is no collimator; instead, the photons impinge on a semiconductor detector (usually germanium) where they undergo Compton scattering and are redirected to a second detector (often a scintillation camera). If the first detector can measure the energy of the Compton event, the scattering angle can be estimated. If both detectors also have 2D spatial resolution, then for each photon we can estimate the angular deviation at the first detector and the line of propagation between the two detectors. This has the effect of localizing the source of the photon to a fuzzy conical shell in the object space. By comparison, a pinhole and one 2D detector localizes the source to a fuzzy ray through the object; therefore, the Compton camera suffers from additional multiplexing around the periphery of the conical shell. This deficiency is compensated to a degree by the improved collection efficiency resulting from omission of the pinhole.

Compton cameras are most suited for high-energy isotopes because the energy loss on scattering increases as the square of the incident energy, and also because the detectors have better relative energy resolution at higher energy. If high-energy isotopes become of interest in small-animal SPECT, Compton cameras should be reconsidered, but for 140 keV and lower, they do not appear to be practical.

3. Detector requirements

Gamma-ray detectors are characterized by their spatial resolution, area, energy resolution, count-rate capability, and sensitivity. We shall discuss each of these performance characteristics in the context of small-animal SPECT, with regard to the different methods of image formation discussed in Section 2.

3.1 Clinical SPECT versus small-animal SPECT

Before getting into specifics on the detector requirements for small-animal SPECT, it is useful to contrast that application with conventional clinical SPECT.

As seen in Table 2.1, the most obvious difference is in the required field of view and spatial resolution; roughly speaking, the field of view for small animals is ten times smaller (in linear dimension), but the resolution must be about ten times finer than for human imaging. When clinical detectors are adapted to animal studies, it is common to use pinholes in order to magnify the image $\sim 10\times$ onto the detector

Table 2.1. Comparison of clinical and small-animal SPECT.

Clinical SPECT	Small-animal SPECT
~ 1 cm resolution	mm or sub-mm resolution
FOV ~ 50 cm	FOV ~ 5 cm
Collimators used to cover FOV	Pinholes used to get magnification
Body dimensions $\gg 1/\mu$	Body dimensions $\ll 1/\mu$
Strong scatter and attenuation	Weaker scatter and attenuation
Multiple scatter likely	Single-scatter approx. more useful
Need $E \geq 100$ keV	Can use $E \sim 30$ keV
Radiation dose critical	Volume of tracer critical
Want half-life \sim hours (e.g., ^{99m}Tc)	Can use longer half-life (e.g., ^{125}I)
General-purpose instruments strongly preferred (commercially)	Adaptable, special-purpose instruments more attractive
Quantitative accuracy desirable (Detection tasks common clinically)	Quantitative accuracy crucial (Estimation tasks needed for research)

face. For more discussion on the use of clinical detectors in small-animal SPECT, see Section 4.2.

Another distinction is that the object being imaged is typically much less scattering and absorbing in small-animal applications than clinically. Of course, the attenuation and scattering coefficients are the same in the two cases, but the body dimensions are different. At 140 keV, for example, the attenuation in soft tissue is almost entirely due to Compton scatter, and the total attenuation coefficient μ is about 0.14 cm^{-1} . Thus, the attenuation length μ^{-1} is about 7 cm, which is large compared to a mouse but small compared to a human. The most probable event in mouse SPECT imaging at 140 keV is that the emitted photon will escape the body with no scattering at all, and multiple scattering is very rare.

The small body dimensions also open up the possibility of using lower-energy isotopes. In particular, ^{125}I is very attractive because many biologically important molecules are available pre-tagged with this tracer. The 60-day half-life makes it possible to order these radiopharmaceuticals ahead of the planned study and to follow the biodistribution over weeks.

Radiation dose is, of course, a critical concern in clinical imaging. It is less important in animal studies so long as it can be established that there are no radiation-induced physiological changes over the period of the study. The more pressing

concern is the physical volume of the injection, which must be restricted to about 0.2 ml for mice. Thus, there is a need for high specific activity, mCi/ml.

In terms of commercial instrumentation, it appears to be the conclusion of most companies in the field that there is no market for specialized instruments that are dedicated to one or a few clinical studies. It is the premise of CGRI, however, that great progress can be made in animal studies by using flexible, modular imaging systems that can be adapted to the needs of specific animal studies.

In terms of task-based performance criteria, there is no difference in principle between clinical and animal systems, but in practice clinical SPECT studies are largely nonquantitative. Great effort has been expended on correcting for scatter, attenuation, and other effects that degrade quantitative accuracy; in most cases, however, the desired clinical outcome is accurate detection or classification rather than quantitation. In research, however, quantitative accuracy is more important, and fortunately the lower attenuation and scatter with small animals facilitates its achievement.

3.2 Spatial resolution

It follows from the considerations in the previous section that excellent resolution is needed for small animals because of the small scale of the details to be imaged. More precisely, as we shall see, high resolution is needed for both detection and estimation tasks.

In addition, certain image-acquisition geometries place great demands on the detector resolution. In particular, the use of multiple pinholes with significant minification, as discussed in Section 2.2.3, requires that the detector resolution be much better than would be needed with 1 : 1 imaging or magnification.

3.2.1 Spatial resolution and lesion detection. Tsui et al. [1978, 1983] were the first to study the effects of spatial resolution on lesion detection in nuclear medicine. They considered detection of a lesion of known size and location superimposed on a uniform but unknown background. They found that the optimum aperture size was approximately equal to the size of the lesion to be detected and that increasing the aperture size beyond this point resulted in reduced detectability despite increased counts.

Numerical and psychophysical studies by Rolland [1990] demonstrated clearly that random inhomogeneities in the background were an important determinant of image quality and of the tradeoff between sensitivity and resolution. Barrett [1990] published a detailed study of the effects of these inhomogeneities on image quality, and Myers et al. [1990] published a study on aperture optimization for planar emission imaging. The conclusion of this latter study was qualitatively similar to that of Tsui et al. [1978]: the optimum aperture resolution is approximately equal to the size of the lesion to be detected. For small, poorly resolved lesions in inhomogeneous backgrounds, however, the improvement in detectability with improvements in aperture resolution could be dramatic. In some cases, a reduction by a factor of two in aperture size could increase the detectability index (SNR^2) by

two orders of magnitude despite the four-fold reduction in counts. These theoretical predictions were verified to a high degree in psychophysical studies [Rolland, 1990; Rolland and Barrett, 1992].

Similar dramatic effects have been noted in PET. Muehllehner [1985] published a series of PET simulations showing that far fewer photons are required for detection of small details if the spatial resolution of the imaging system can be improved. He arrived at the rule of thumb that, for every 2 mm improvement in detector spatial resolution (in the range 4 – 14 mm), the total number of counts can be reduced by a factor of three to four for equal subjective image quality.

These studies all show that small improvements in spatial resolution can result in a large improvement in objective performance measures. Theoretical studies such as Wagner and Brown [1985] and Barrett [1990] make it clear that aperture and detector resolution are much more important than post-detection image reconstruction or processing. Resolution improvements achieved algorithmically are irrelevant to an ideal observer. For the human observer, algorithmic resolution variations have a small effect [Abbey and Barrett, 1995; Abbey, 1996], but the real leverage is in the design of the detection system.

3.2.2 Spatial resolution and estimation tasks. Similar conclusions hold for estimation tasks. Consider the common task of estimating the activity of a tracer in some region of interest (ROI). This task is usually performed simply by manually outlining the region on a reconstructed image and then adding up the grey values in the region defined this way. Many factors, including scatter and attenuation, contribute to the errors in the resulting estimate, but even if these factors are controlled, there is still the effect of the finite spatial resolution. A bright source outside the region of interest can contribute to the sum of grey values within the region because of tails on the point spread function. In fact, the bias in the estimate is a strong function of the object distribution *outside* the region, and it is impossible even to define an estimator that is unbiased for all true values of the parameter [Barrett and Myers, 2004, Chapter 13].

There are two ways of ameliorating this effect. The first is to use an estimator that explicitly takes into account the detector resolution as well as the noise statistics [Barrett, 1990]. The second, and much better, approach is to improve the system resolution.

Other estimation tasks also benefit from improved resolution. For example, in a careful study of optimal collimator selection for estimation of tumor volume and location, Müller et al. [1986] found that collimators designed for high resolution, even at substantial cost in sensitivity, would lead to significant improvements for brain SPECT.

3.2.3 Specifying the resolution. For both detection and classification tasks, the fundamental limitation is the resolution associated with the hardware — the collimator and detector. The resolution contribution from the algorithm has no effect at all on task performance if the task is performed optimally. For suboptimal

observers, such as a human reading the image or a simple ROI estimator, the algorithm indeed plays a role, but that may point to the need for better observers rather than better reconstruction algorithms. For example, a computer-assisted diagnosis algorithm can in principle be designed to overcome the limitations of the human in detection tasks, and optimal estimators can be designed to extract the desired quantitative parameters.

Thus, at a fundamental level, the best way of specifying system resolution is in terms of the hardware only, without reference to any particular reconstruction algorithm. One way of doing this is to use the Fourier cross-talk matrix [Barrett and Gifford, 1994; Barrett, 1995a, 1996] which makes it possible to define a kind of modulation transfer function for systems that are not even approximately shift-invariant. The Fourier cross-talk matrix is an exact description of the deterministic properties of any linear digital imaging system. It is independent of the task the system must perform, but methods developed in Barrett et al. [1995a] can be used to compute task performance from the cross-talk matrix and information about the measurement noise.

Another reason not to include the algorithm in specifications of resolution is that the final point spread function (PSF) in a reconstructed image can be varied over a wide range by setting reconstruction parameters such as smoothing factors, number of iterations and voxel size. With accurate modeling and iterative reconstruction, one can obtain almost arbitrary reconstructed resolution, generally at the expense of noise although not necessarily at the expense of task performance. Thus, it is highly misleading to state “the resolution” of a system that includes a reconstruction step.

Moreover, when resolution is specified in tomographic imaging, it is necessary to distinguish volumetric and linear resolution. A linear resolution of about 1 mm is obtainable these days in both animal PET and animal SPECT; if this resolution is obtained isotropically, it corresponds to a volume resolution of about 1 μL , legitimizing the terms microPET and microSPECT. It is really the volumetric resolution, mainly of the hardware, that determines the limitation on task-based image quality for either detection or estimation tasks.

3.2.4 Pixellated versus continuous detectors. As we shall see below, two distinct kinds of scintillation detectors are used in SPECT (and also in PET, although we shall have very little to say about PET detectors). One kind uses a monolithic detector like the large NaI crystal used in clinical Anger cameras. The other kind of detector, favored in small-animal systems based on position-sensitive photomultipliers (PSPM Ts), uses a segmented or pixellated crystal. In decision-theoretic terms, the data-processing task with monolithic crystals is to estimate the position of the scintillation event on a continuous scale, binning the estimate into discrete pixels for storage and display only. With the segmented crystals, the data processing must decide in which segment the event occurred, thus performing a classification task rather than an estimation task.

A similar situation arises with semiconductor detectors. Discrete arrays of individual elements are a quick way of constructing imaging detectors, but the complex-

ity and cost of the systems increase rapidly with the number of elements. To avoid these problems, monolithic semiconductor crystals are used with discrete electrodes (see Section 5.2).

The question then arises as to how to specify and compare the resolutions of these two distinct kinds of detectors. The common approach is to use the segment size as the resolution measure in pixellated detectors and the full width at half maximum (FWHM) of the detector PSF as the measure for monolithic detectors.

This approach is unsatisfactory for two reasons. First, it takes no account of the task the system is expected to perform. Second, the distinction between the two kinds of detector is really a false dichotomy. Consider a monolithic semiconductor crystal with a discrete array of small electrodes. Is this a pixellated detector? It is if the location of the event is estimated, as it commonly is, by the address of the electrode that receives the largest amount of charge. On the other hand, the discrete electrodes are no different in principle from the discrete PMTs in an Anger camera, and one event gives a signal in multiple electrodes, therefore position estimation on a continuous scale can be performed as well. The size of the electrode is no more a resolution limitation than is the size of a PMT in an Anger camera.

These points will be discussed in more detail in the next chapter where we cover optimal approaches to position estimation with both semiconductor and scintillation detectors.

3.2.5 3D detectors. So far, we have discussed detector resolution as if it were associated with the 2D response of the detector. For many purposes, however, the detector is required to sense the position of the gamma-ray event in 3D. Consider, for example, a simple pinhole imaging system where the pinhole is placed close to an extended object. Then some of the photons from the object pass through the pinhole at oblique angles, up to 45° or more, and hence impinge on the detector at the same angle. Because gamma-ray detectors necessarily have a finite thickness in order to absorb the photons, the 3D location of the interaction event must be determined in order to accurately estimate the path of the photon. In other words, the detector must provide information about the depth of the interaction as well as its lateral position.

Many schemes are found in the literature for increasing the sensitivity of a gamma-ray detector to depth of interaction. Whatever scheme is used, the maximum-likelihood methods to be presented in Chapter 3 can be used to estimate the 3D coordinates of the interaction.

3.3 Detector area and space-bandwidth product

Another key parameter of a detector is its physical area. With a parallel-bore collimator, the area of the detector directly determines the field of view. With pinhole imaging, however, area alone is not what matters. A large-area, low-resolution detector can be used at large magnification to achieve the same field of view and

final resolution as a small-area, high-resolution detector used at lower magnification (see Fig. 2.1).

The total number of independent measurements that the detector can make is what really matters. For a discrete detector array, that number is the number of individual elements in the array. For a continuous detector such as an Anger camera, the maximum number of independent measurements that can be made can be approximated by the area of the detector divided by the area associated with the PSF after position estimation. Because the reciprocal of the width of the PSF is a measure of width of the modulation transfer function (for a shift-invariant system), we can say that the important quantity in detector performance is the *space-bandwidth product*, defined by

$$\begin{aligned}\text{Sp-BW} &= (\text{Area of detector}) / (\text{Area of PSF}) \\ &= (\text{Area of detector}) \times (\text{2D bandwidth}).\end{aligned}\tag{2.5}$$

A larger detector is of no use if the image does not fill the detector area. In a statement probably attributable to W. L. Rogers, pinholes and coded apertures are simply ways of taking advantage of the available detector space-bandwidth product. The arguments presented in Section 2.2.3 show how an increase in either the resolution or the area of the detector can be used to increase the performance of a multiple-pinhole system without multiplexing; if the object has a sparse structure, so that relatively few detector elements receive significant radiation, then further advancement can be achieved with multiplexing.

3.4 Energy resolution

Most gamma-ray detectors have the ability to estimate the energy deposited in an interaction event as well as the position of the interaction. Note the wording: The detector does not estimate the energy of the *photon*, and in any case it provides only an *estimate* rather than an unambiguous determination of the energy it senses.

This energy estimate has two main uses. First, if two separate isotopes are used in a study, the energy information provides data needed to reconstruct two separate images; accuracy of the energy estimate determines the degree of influence one isotope distribution has on the reconstructed image of the other distribution.

The energy estimate also is used to discriminate against photons that have undergone Compton scatter in the patient's body, on the assumption that scattered photons carry little spatial information and hence degrade system performance. Whether this assumption is valid is an interesting question, discussed briefly in Section 3.4.2 after we look at scatter discrimination in small-animal imaging.

3.4.1 Energy resolution and scatter discrimination. As noted in Section 3.1, Compton scattering is not as strong in small-animal studies as it is clinically because the body dimensions are so much smaller. How important the residual scatter is depends, of course, on the task and observer. For now, let us assume that the scatter is undesirable and see what can be done about it.

The effectiveness of energy discrimination in rejecting scatter depends on the energy of source, on the energy resolution of detector, and on a choice the user makes in setting the tradeoff between rejecting scattered photons and rejecting the presumably desirable unscattered photons.

As a numerical example, the resolution of typical scintillation detectors at 140 keV, as measured by the FWHM of the distribution of energy estimates, is about 15 keV. High-atomic-number, room-temperature semiconductor detectors such as cadmium zinc telluride (CZT) can have energy resolutions of order 2–3 keV as single elements and 6–8 keV as imaging arrays. For comparison, a 45° Compton scatter at 140 keV produces an energy loss $\Delta E = 10$ keV. Thus a CZT detector is superior to a scintillation camera for scatter rejection with ^{99m}Tc , but neither is perfect.

There also is considerable interest in small-animal imaging with ^{125}I , which has several emission lines in the vicinity of 30 keV. At that energy, a 45° scatter yields an energy loss $\Delta E = 0.5$ keV. Neither scintillation detectors nor CZT detectors offer much chance of scatter discrimination in this case.

Silicon detectors are attractive at 30 keV, and the best single-element silicon devices can give resolutions less than 1 keV. Even this is not really good enough, however, because the gamma-ray emission of ^{125}I is not monoenergetic to start with, and silicon imaging arrays have much poorer energy resolution than single-element detectors in any case.

Whatever the energy resolution of the detector, the user must employ some algorithm to discriminate scattered from unscattered radiation. If that decision is to be made for each event in isolation, as it usually is, then the only information for making the decision is the energy estimate. The conventional — though scarcely optimal — approach is simply to compare the energy estimate to a threshold and make the decision to accept the event if the estimate exceeds the threshold. (An upper threshold can also be used but it isn't relevant to scatter rejection because Compton processes always result in energy loss.) Setting the threshold too high results in rejecting too many unscattered photons, while setting it too low results in accepting too many scattered photons.

To study this tradeoff, Jyh-Cheng Chen [1997] used a kind of receiver operating characteristic (ROC) curve in which the probability of accepting an unscattered photon (true positive) is plotted vs. the probability of accepting a scattered photon (false positive). He used this kind of plot to compare different methods of energy estimation and to choose a setting of the threshold.

We shall return to issues of energy estimation and scatter rejection in Chapter 3.

3.4.2 Energy information and task performance. The importance of scattered radiation in SPECT imaging depends on the task and observer and on the reconstruction algorithm, as well as on any scatter-discrimination method used.

For simple detection tasks in uniform backgrounds, White [1994] found that best ideal-observer performance was obtained with a wide-open energy window; the increased acceptance of unscattered photons outweighed the degradation due to

scatter. For a similar task, Rolland et al. [1989, 1991] showed that the long tails of the scatter PSF degraded human performance but that much of the effect could be recovered by simple linear deconvolution. Unpublished work by White and Gallas indicates that the similar conclusions may hold for detection in a more complicated background: there might not be much of a penalty in detection task performance when a wide energy window is used.

There may even be some benefit to collecting scattered radiation, estimating the energies, and using this augmented data set for detection. Kwo et al. [1991] studied this possibility for intraoperative tumor detection, a setting similar to small-animal imaging in that the lesion can be rather close to the detector. They found that detection performance for an ideal linear (Hotelling) observer increased when the scattered photons were used optimally. They also showed that HgI₂ and CdTe semiconductor detectors offered some advantage over NaI(Tl), not for scatter rejection but for providing more accurate energy information to the observer. For more on optimal use of scattered radiation, see Barrett et al. [1998].

3.5 Count-rate capability

Traditionally, one of the main limitations of gamma cameras has been the count-rate capability. Depending on the technology, modern cameras show a loss in sensitivity or degradation of resolution when the count rate exceeds 100,000 – 200,000 cps. The problems only become more serious for small-animal imaging where the desire for high spatial resolution and reasonable imaging times often leads to injection of large amounts of activity, all of which can end up in the field of view of the detectors. Moreover, the high collection efficiency of coded apertures and multiple-pinhole systems leads to still higher count rates.

3.5.1 Modularity. Although improvements in electronics are always desirable, the best way to deal with high total count rates is with multiple independent camera modules. Although this approach is used clinically, with 2, 3, or even 4 camera heads, it is possible to use many more in small-animal SPECT. Of the systems being developed at CGRI (see Chapter 6), FastSPECT uses 24 modules, FastSPECT II uses 16, and SemiSPECT currently uses 8 modules but can be upgraded to 16. A system with N independent modules automatically has N times the count-rate capability (not to mention N times the sensitivity) of an otherwise identical system with a single module.

Other practical advantages of modular systems include the low cost of individual modules, the ease of troubleshooting and repair, and the flexibility in rearranging the modules for different applications.

3.5.2 Rationale for counting. Another way to deal with the demands of high count rates is to just say no – to use an integrating detector instead of a photon-counting one. Integrating detectors are the standard in digital radiography, where it is very difficult to build counting arrays that will have adequate speed. Why not just use these same detectors for nuclear medicine? We shall have more to say about

this question in Section 4.2.2, but for now we simply enumerate the reasons for doing counting in the first place.

One reason for photon counting is so we can do energy discrimination and hence scatter rejection. We argued above, however, that scatter was not all that important in degrading small-animal SPECT images, so this reason for counting is not compelling.

The second reason for counting is that different absorbed gamma rays produce different pulse heights, because of Compton scatter in the body or detector, escape of K x-rays from the detector, or absorption or scattering in the detector material itself. With a photon-counting detector, these pulses are analyzed individually and accepted or rejected for inclusion in the image. No matter what the acceptance criterion is, the resulting image will obey Poisson statistics [Barrett and Myers, 2004]. With integrating detectors, however, each pulse makes a contribution to the image proportional to the pulse height, and the random variation in pulse height produces an additional noise often called Swank noise, after the person who first analyzed it. We shall discuss Swank noise in more detail in Chapter 3, but for now we merely note that it is seldom more than a 20% increase in noise variance above the Poisson level.

The final reason for counting is that integrating detectors have additional noise contributions arising from dark current and thermal noise in the readout electronics. For more on these noise sources and ways of controlling them, see Section 4.2.2.

3.5.3 Counting with an integrating detector. The distinction between photon-counting and integrating detectors is another false dichotomy. Depending on the rate of arrival of photons and the frame rate, it may well be possible to identify the effects of individual photons in each frame from an integrating detector. Furenlid et al. [2000] analyzed the statistics of this process and determined the allowable count rate as a function of the frame rate, the number of detector pixels affected by each gamma-ray photon, and the allowable degree of overlap.

We shall return to this question several times below, in the context of integrating arrays of semiconductor detectors and of lens-coupled CCD cameras.

3.6 Sensitivity

For a photon-counting device, the detector efficiency is defined as the fraction of incident photons that are counted; in other words, it is the fraction absorbed multiplied by the probability of being counted through the energy window or other thresholding means. Often the term *photopeak efficiency* is used. This quantity is to be contrasted with the overall system efficiency which also includes the probability that an emitted photon will pass through the imaging aperture.

In system design, we may trade absorption efficiency for spatial resolution (e.g., by using thinner crystals), but then obtain the overall sensitivity back, say by use of multiple pinholes. When this possibility is considered, a useful figure of merit for

the detector is the space-bandwidth-efficiency product, defined as

$$\text{FOM} = \frac{\text{Area of Detector}}{\text{Area of resolution cell}} \times \text{Detector efficiency.} \quad (2.6)$$

4. Approaches to gamma-ray detection

Having established the general characteristics, we wish to achieve in detectors for small-animal SPECT, we now look broadly at how we might go about achieving them. In this section, we consider the nature of the initial interaction between the gamma ray and the detector material and ways of sensing the effect of that interaction, possibilities for adapting existing clinical detectors to small-animal SPECT, and some of the advantages of dedicated small-animal detectors.

4.1 The initial interaction

The inelastic interaction of sub-MeV gamma rays with matter takes place by the photoelectric effect or Compton scattering. In both cases, the result is that a high-energy electron is produced in the material. Different detector technologies are distinguished by how they sense this initial interaction. To see what the options are, we examine the events that occur in any nonmetallic material after the interaction.

4.1.1 Cascades. After production of a high-energy electron, there is a complicated cascade of events. The high-energy electron can excite lattice vibrations (mainly optical phonons), and it can also produce hole-electron pairs by exciting electrons across the band gap. The holes and electrons can be very energetic; that is, the electron energy might be far above the bottom of the conduction band and the hole might be far below the top of the valence band. The holes and electrons lose energy either by producing phonons or by exciting other hole-electron pairs.

After they have lost most of their energy, the holes and electrons can bind together to form excitons, and they eventually recombine, often through the intermediary of impurities. The recombination can be *radiative*, meaning that low-energy optical photons are produced, or *nonradiative*, meaning that the energy is dissipated through phonons.

In addition to the high-energy electron, the initial gamma-ray interaction also produces one or more high-energy photons. If the initial event is Compton scattering, the scattered gamma ray may escape from the crystal, or it can be absorbed or scattered at a second location, producing another high-energy electron and starting a similar cascade of hole-electron production at that location. Similarly, if the initial event is photoelectric, it leaves a vacancy in an inner shell of the atom it interacts with, and this vacancy is filled by production of a characteristic x ray. Like the Compton-scattered photon, this x ray can escape the crystal, or it can interact and start another cascade.

The cascades of events produce charge (holes and electrons), light (optical photons) and heat (phonons); any of these products can be used to transduce the initial interaction into a signal in an external circuit. Semiconductor detectors sense the charge, scintillation detectors sense the light, and microbolometers or superconductors sense the heat.

4.1.2 Nonlocality. As the spatial resolution of gamma-ray detectors improves, it becomes relevant to inquire about the spatial scale of the events described in Section 4.1.1. For numerical illustration, we consider a CZT detector and a 140 keV gamma ray, but the scales will be similar for other detectors.

For this material and gamma-ray energy, the attenuation length is about 2.5 mm; hence, the detector thickness must also be near this value to obtain reasonable absorption efficiency. If the 140 keV gamma ray interacts photoelectrically with the K shell of one of the constituents of CZT, it produces a photoelectron of energy around 100–120 keV, depending on whether the interaction is with cadmium, tellurium, or zinc. The range of this photoelectron is of order $20\ \mu\text{m}$, and this dimension specifies the size of the distribution of the hole-electron pairs, and hence also that of the light distribution for the radiative recombination. The range of the K x ray is around $100\ \mu\text{m}$, again depending on which constituent it comes from; because this number is small compared to typical detector thicknesses, it is highly likely that the x ray will be reabsorbed.

The ranges of the photoelectron and K x ray are comparable to the detector resolution we would like to achieve. At CGRI, we have built CZT detectors with pixels as small as $125\ \mu\text{m}$ and silicon detectors with $50\ \mu\text{m}$ pixels.

4.2 Clinical detectors

Next we investigate the prospects for using available clinical detectors for small-animal SPECT. Both clinical scintillation cameras and detectors developed for digital radiography will be discussed.

4.2.1 Clinical scintillation cameras. Clinical scintillation cameras are bulky and expensive, and they do not provide the flexibility needed for optimal small-animal SPECT. The spatial resolution is typically around 3 mm at 140 keV, but they do have respectable space-bandwidth products, around 20,000 per detector head, because of their large area.

In practice, there may be some difficulty in utilizing the available detector area. If we attempt to use the edges of the camera with pinholes at large magnification, we encounter an additional problem: rays arriving at the edges do so at an oblique angle, and clinical cameras do not have depth resolution; therefore, the effective spatial resolution is degraded.

As noted above, there is considerable interest in small-animal SPECT with the 30 keV radiation from ^{125}I , and commercial cameras do not work well at this energy. Some of them do not even permit setting the energy window this low. Those that do will inevitably have poor spatial resolution because the light output in any scintillator

is proportional to the photon energy; 30 keV gamma-ray photons produce less than one quarter the light of 140 keV photons, and thus have a point spread function that is over twice as wide.

Nevertheless, numerous groups are making very good use of commercial scintillation cameras with small pinholes placed very close to a mouse or rat. Several of the contributed papers in this volume describe the state-of-the-art in this endeavor.

4.2.2 Digital-radiography detectors. X-ray detectors for digital radiography (DR) are an active area of research, and several viable technologies have appeared. The most promising at this writing appear to be amorphous selenium layers and CsI scintillators with photodiode readouts, but detectors based on polycrystalline PbI_2 and HgI_2 layers also are getting serious attention.

For our purposes, DR detectors are attractive because of their high space-bandwidth product. Digital mammography detectors, in particular, must have high spatial resolution (50–100 μm), and they have a convenient size for imaging mice and rats.

The active layers in these detectors are usually rather thin (100–200 μm), which is good for pinhole SPECT because it minimizes blurring for photons arriving at oblique angles, but bad for higher-energy applications because the efficiency is reduced. As argued in Section 3.6, however, it is often advantageous to trade efficiency for space-bandwidth product.

The most salient property of DR detectors, however, is that they operate in an integrating mode instead of photon counting. As noted above, this means that there is excess noise arising from the readout electronics, dark current, and pulse-height variations. In SPECT applications, dark current and electronic noise can be minimized if the frames are read out rapidly and if an individual threshold is applied to each frame. The idea is that an individual gamma ray produces high-amplitude signals confined to a few detector pixels, while electronic noise and dark current give low-amplitude signals in all pixels. Depending on the signal levels, it may be possible to choose a threshold such that the excess noise is effectively eliminated, provided that only a few photons are detected in each frame. It must be noted, however, that because rapid frame rates require higher electronic bandwidths and hence yield higher read noise, the success of this strategy will depend on the characteristics of the particular DR detector as well as on the arrival rates and energies of the gamma rays.

As we shall see in Chapter 3, Swank noise is probably not a serious limitation in using DR detectors for small-animal SPECT, but if it is, it can be eliminated by a similar frame-by-frame analysis. Each frame can be analyzed to determine the locations of gamma-ray events, and the random pulse amplitudes can be replaced by constant signals at those locations. The resulting image statistics will be purely Poisson, with no remaining excess noise.

4.3 Dedicated small-animal detectors

4.3.1 Objectives. Even though clinical gamma cameras and digital-radiography detectors are applicable to small-animal SPECT, there is still considerable motivation for developing dedicated gamma-ray detectors for this application. The goals of this endeavor are to produce inexpensive, high-resolution modules that are well suited to small animals. Such modules would allow considerable flexibility in system design and optimization. If each module has a high resolution and many modules can be placed in close proximity to the animal, a large effective space-bandwidth product can be achieved.

Moreover, with many modules and many pinholes, all of the projection data needed for tomographic reconstruction can be obtained in parallel, with no motion of the animal or the imaging system. As with the FastSPECT systems developed at CGRI, this opens up the possibility of true 4D imaging, i.e., 3D tomography with no inherent limitation in temporal resolution.

4.3.2 Current technologies. In addition to CGRI, several other laboratories are developing gamma-ray detectors, especially for small-animal SPECT. The devices receiving the most attention at this writing are based on either scintillation crystals or semiconductors. Scintillation devices under investigation include modular scintillation cameras, scintillation cameras based on multi-anode photomultiplier tubes, and discrete arrays of small photodiodes. Semiconductor detectors of current interest are either arrays of discrete elements or integrated (“hybrid”) devices in which a slab of semiconductor material is bonded in some way to one or more application-specific integrated circuits (ASICs) for readout.

More details on semiconductor and scintillation detectors will be given in Sections 5 and 6, respectively.

4.3.3 Other potential detector technologies.

Proportional counters. In a gas, constant-gain ion multiplication can be achieved within a range of electric field strengths denoted by the proportionality region, see Knoll [1999]. Ion multiplication (termed Townsend Avalanche) results from the large mean free path of the electrons. Above a critical field strength, the free electrons gain enough energy to ionize additional gas molecules before they collide. The heavier ions have a larger interaction cross section and do not gain enough energy between collisions to ionize other molecules.

Proportional counters are useful in detection and spectroscopy of low-energy x-radiation (2–60 keV). Energy resolution is typically about 15%, and time resolution is about 1 μ sec, which is comparable to the performance of lithium-drifted silicon detectors for these energies. However, energy resolution can be very sensitive to nonuniformities of the ionization chamber and of the anode wire. In addition, instabilities in the gas can result in spurious pulses. Finally, conventional proportional counter chambers are relatively large for use in small-animal imaging.

Gas-electron multiplication (GEM) device. Building on the concept of gas-ionizing detectors, a number of groups have developed alternative methods to generate position- and energy-sensitive devices capable of single-photon detection and imaging. One of the more recent of these gas-ionizing detectors is the GEM. A GEM detector consists of metal-insulator-metal foil with an array of double conical, hourglass holes drilled through the foil. The foil is suspended in a gas-filled chamber between two electrodes with an applied potential, divided across the electrodes and the GEM metal layers. Ionized electrons accelerate and converge on the holes, where the electric field intensifies, causing charge multiplication. The amplified charge pulse then passes out of the foil, where it transfers to either another GEM layer or to collection electrodes. Most ions generated in the avalanche region drift along field lines away from the holes, mitigating the charge buildup on the insulating layer.

GEM devices can be built in large or small areas and with a fine pitch between holes ($\sim 100\mu\text{m}$ pitch with $\sim 50\mu\text{m}$ diameter holes). However, as with all gas detectors, the sensitivity to noncharged radiation such as x-ray or gamma-ray sources is small unless a thick gas layer is used, reducing the spatial resolution. One alternative that has recently been pursued is to hybridize this technology with a photocathode and a scintillator to improve the sensitivity of the device to gamma rays and x rays; see Breskin et al. [2002] and Mörmann et al. [2002]. This technique is now in competition with flat-panel, multi-anode photomultipliers that have recently been developed.

Micro-arrays of Superconducting Tunnel Junctions (STJ). Interaction of radiation with the superconducting electrodes of an STJ produces excited states of the superconducting Cooper pairs, referred to as quasiparticles. The energy gap for the quasiparticle excitations in a superconductor is small ($\sim 1\text{ meV}$), which results in three orders of magnitude more charge carriers per incident photon than with conventional semiconductor detectors. Consequently, an STJ is very sensitive to variations of energy of the incident radiation. With a bias applied, these quasiparticles tunnel through the insulating barrier, generating a current pulse with amplitude proportional to the absorbed energy. With excellent energy resolution (5 eV for radiation for energies below 1 keV) and good temporal resolution ($10\mu\text{sec}$), these compact devices are capable of simultaneous imaging and spectroscopy. However, STJ sensitivity falls off at higher energies ($> 10\text{ keV}$), and cryogenic cooling is required.

Photostimulable phosphors (PSPs). PSPs store energy from absorbed x rays by trapping generated electron-hole pairs in impurity levels deep within the bandgap of the crystal. The depth of the trap makes thermal detrapping unlikely. The distribution of the deposited energy can later be read out and digitized by scanning a focused laser over a PSP. Trapped charge carriers are re-excited and can recombine with some probability. In this way, the stored energy is read out, one pixel at a time. Resolution is typically limited by the spot size of the laser and by diffusion of laser

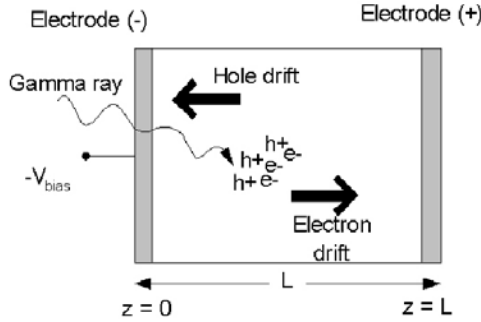


Figure 2.5. Basic principle of a single-element semiconductor detector.

light into the PSP. Because radiation fluence is integrated in the PSP, identification and counting of individual events is not possible. Limits in sensitivity (or resolution for thicker phosphor plates), and the requirement to scan the plate after each projection, make this method a slow and generally noncompetitive technology for use in SPECT.

5. Semiconductor detectors

A brief introduction to semiconductor detectors is provided in this section. Topics discussed include the basic physics of charge generation and transport, device configurations for imaging, and the considerations in the choice of materials.

5.1 Charge generation and transport

The operation of a simple single-element (nonimaging) semiconductor detector is illustrated in Fig. 2.5. As discussed in Section 4.1, the gamma ray undergoes a photoelectric or Compton interaction and produces a high-energy electron, which subsequently dissipates its energy by generating lattice vibrations (phonons) and charge (holes and electrons). Semiconductor detectors operate by sensing the presence of the charge.

5.1.1 Mobility and trapping. When a bias voltage is applied to the semiconductor detector shown in Fig. 2.5, it creates an electric field in the interior of the material. The field distribution depends on the nature of the electrode contacts and the bias voltage. If blocking (diode-like) electrodes are used, and the bias is high enough, then any free carriers that might arise from thermal excitation are swept out and the device is said to be *fully depleted*. It is also useful to assume that the transverse dimensions of the crystal are large compared to its thickness and that the material is homogeneous. If all of these assumptions are valid, the electric field in the device is uniform, just as it would be in a dielectric-filled plane-parallel capacitor.

The electrons in this uniform field move toward the anode, while the positively charged holes move toward the cathode. Because of interactions with phonons and impurities, however, the holes and electrons do not accelerate indefinitely but quickly reach a terminal velocity related to the field. For sufficiently small fields, the terminal velocity v is simply proportional to the field E . We call the constant of proportionality the mobility and denote it as μ , so $v = \mu E$. Practical units of μ are (cm/sec)/(Volts/cm) or cm²/Volt-sec. As an example, in CZT, μ for electrons is around 1000 cm²/Volt-sec and for holes it is about 100 cm²/Volt-sec.

When they are free, the electrons and holes move at their respective drift velocities μE , but they can also be trapped at sites of impurities or lattice defects. If they remain free for a mean time τ , they move a mean distance $\nu\tau$ or $\mu\tau E$. After trapping, the carriers can be detrapped by thermal excitation or they can recombine. It is often assumed that, if detrapping occurs, it does so on a long time scale when compared to the measurement time of the electronics and can hence be neglected.

5.1.2 Charge induction. One might think that the carriers would need to drift to the electrodes to be observable, but in fact any motion of the carriers within the material induces a time-varying charge on the electrodes and hence an observable current in the external circuit. One way to see why this is so is to recognize that the bias circuit holds the potentials on the electrodes at constant values; for example, as shown in Fig. 2.5, the anode is held at 0 V. Thus, a negative point charge within the interior must be balanced by a fictitious positive image charge an equal distance on the other side of the anode, and it is the movement of this image charge that is sensed as a current. More physically, the actual negative charge draws charge from the circuit in such a way that a net positive distribution of surface charge on the anode is induced, maintaining the anode at ground potential.

5.2 Imaging arrays

5.2.1 Types of arrays. The simplest way to make an imaging semiconductor detector is to produce N individual detectors, of the type shown in Fig. 2.5, and mount them in a regular array to yield a discrete image detector with N pixels. For large N , this approach is costly because it requires N separate detectors and N sets of electronics.

Another approach is to start with a monolithic slab of semiconductor material, deposit electrodes on both sides, and use photolithography to partition one or both of the electrodes into separate channels. If, say, the cathode is left unpartitioned but the anode is divided into a regular array of N pixels, then electrically the system is similar to an array of N individual detectors, but mechanically it is much easier to construct. This type of device still requires N sets of electronics.

An alternative to pixel arrays is to use a semiconductor detector with orthogonal strip electrodes on opposite faces and synthesize pixels by detecting coincident signals on the row and column strips [McCready, 1971]. This approach has been used with CZT by a number of gamma-ray astrophysics research groups [Ryan, 1995; Stahle, 1996; Matteson, 1997]. The largest of these devices, the BASIS array

built at NASA Goddard Space Flight Center [Stahle, 1997], has more than 5×10^5 defined pixels.

Many other clever electrode schemes have been suggested. Some have as their objective overcoming the effects of charge trapping, while others are intended to give more information about the depth of interaction.

5.2.2 Application-specific integrated circuits. Modern semiconductor detector arrays almost always use application-specific integrated integrated circuits (ASICs) for the readout electronics, thereby greatly reducing the cost per channel.

There is considerable variability in the specific circuitry implemented on each channel, but two general categories can be identified. The first is *event-driven electronics*, in which the presence of a gamma-ray interaction is recognized, and some characteristics of the resulting pulse are measured. The second is *integrating electronics*, in which the signal from each electrode is integrated over a fixed period, whether or not an event occurs.

In Section 3.5.3 we briefly mentioned the use of an integrator to detect individual gamma rays and measure their energy, and this approach can work very well with pixellated semiconductor arrays. With readout times of order one millisecond, a pixel rarely contains more than one gamma-ray hit, and individual events are easily identified and segmented.

A drawback to integrating detectors is that they integrate not only the current resulting from gamma-ray events but also the leakage current inherent in semiconductors. This current, which adds noise to the signals and degrades the energy resolution, can be reduced by using higher-resistivity material, cooling the device, or reducing the electric field; the latter is undesirable because it also reduces the drift lengths ($\mu\tau E$) for holes and electrons.

5.2.3 Charge spreading and induction in arrays. As we have emphasized above, it is highly desirable to have imaging detectors with high spatial resolution and large space-bandwidth product, but small pixels lead to interesting problems with semiconductor arrays.

Consider again a CZT detector for 140 keV photons. As noted in Section 4.1.2, the detector thickness t must be around 2–3 mm to obtain good absorption efficiency; yet, we would like to have detector resolutions of 0.5 mm or less for small-animal SPECT. At CGRI, we have built CZT arrays with pixels as small as 0.125 mm, and our standard semiconductor detector uses 0.380 mm pixels. The aspect ratio (material thickness t divided by pixel width w) is in the range 5–20.

It would make little sense to use such aspect ratios for photodetectors in conventional scintillation cameras because the light would spread by an amount comparable to the thickness as it propagated to the photodetector plane. In semiconductors, however, the charge carriers tend to follow the field lines; ideally, all carriers generated by a gamma ray would be drawn to the electrodes along paths perpendicular to the electrode planes, and charge would be collected in only one detector pixel for each interaction.

In reality, there are several mechanisms for sharing charge among multiple pixels. The initial interaction produces a compact cloud of holes and electrons, and there is charge diffusion driven by the concentration gradients that causes the cloud diameter to grow with time. Moreover, once the holes and electrons have separated, there is a Coulomb repulsion that tends to spread the clouds further. When this cloud of charge arrives at an electrode plane segmented into small pixels or small strips, each event can produce signals in several output channels.

Another effect that can cause charge sharing is trapping. Suppose there is no diffusion or Coulomb repulsion, so that each carrier is drawn in a straight line toward the electrode plane, but that many of the carriers are trapped before reaching the plane. The effect of the trapped charge on different pixels is described by something called the *weighting potential* associated with that pixel, but the net effect is that one event can give signals in several pixels. See Eskin et al. [1999] and references cited there for details on calculating the weighting potential and analyzing its effect. Additional discussion can also be found in Barrett and Myers [2004, Chapter 12].

5.2.4 Small-pixel effect. The weighting potential associated with small pixels can be put to good use with CZT and other materials in which electron transport is much better than hole transport. Often the drift length for electrons is large compared to the detector thickness, $\mu_e \tau_e E \gg t$; hence, the electrons readily propagate all the way across the detector. For holes, however, it is often the case that $\mu_h \tau_h E \ll t$; thus, holes have a high probability of being trapped before traversing the detector.

The impact of hole trapping depends on the size of the pixel and the detector thickness. For a pixel of width w , the weighting potential extends to a distance of order w into the material. If $w \gg t$, as it is in typical single-element detectors, then the pixel is equally sensitive to carriers at all distances from the pixel, and the total effect of any carrier depends on how far it moves. If the interaction occurs near the cathode, holes can make it to their collecting electrode and give their full contribution to the output signal. For interactions nearer the anode, however, the holes make a smaller contribution; therefore, the overall signal is strongly dependent on depth of interaction, with severe degradation in the pulse-height spectrum.

With small pixels ($w \ll t$), this effect can be greatly ameliorated simply by making the pixels the anodes. The pixels are sensitive mainly to carriers that move to within w of the anode plane. Because electrons are unlikely to be trapped, they move into this sensitive region no matter where they are produced, but holes move away from the anode pixel, thus, hole trapping is almost irrelevant.

This so-called *small-pixel effect* [Barrett, 1995b] can have a dramatic impact on the pulse-height spectrum, with many more of the events concentrated in the photopeak. If the pixel width w is made too small, however, diffusion and Coulomb repulsion come into play, and the pulse-height spectrum is again degraded. For CZT, the optimal pixel size for a single-pixel spectrum is around 0.5 mm [Eskin, 1999], which is very convenient for small-animal SPECT.

On the other hand, Marks et al. [1999] showed that significant improvements in energy resolution can be obtained for much smaller pixels if multiple pixel signals are used in the energy estimation. Integrating detectors are particularly convenient if this kind of processing is anticipated, because it is straightforward to read out the signals on several contiguous pixels.

5.3 Materials

5.3.1 Desirable material properties. From the above discussions, we can readily compile a list of the properties we would like to have in an ideal semiconductor material for use in small-animal SPECT.

The material also should have high gamma-ray absorption, which means it should have high density and high atomic number. Compounds of Pb, Hg, and Tl are particularly attractive in this regard.

The material should have high resistivity at room temperature, which necessitates both high bandgap and low impurity density. High resistivity is especially important if the material is to be used with an integrating detector. The resistivity requirement is reduced with event-driven electronics which do not integrate the leakage current or with system designs that permit modest cooling.

The material should exhibit good charge transport, with high mobility and low trapping, which in turn requires homogeneous, defect-free crystals. Because mobility and trapping time are only weak functions of temperature in most materials of interest, cooling does not help the charge transport appreciably.

Of course, low cost is always of interest, but especially so when large-space-bandwidth products are desired. If the cost per unit area of the material is high, or large crystals are simply not available, it may be economically prohibitive to fabricate large-area detectors. Small-animal SPECT has an advantage over clinical SPECT because the required field of view is less, and an increased space-bandwidth product can be achieved with smaller pixels rather than a larger detector area.

5.3.2 Candidate materials. A few of the materials that have been investigated as gamma-ray detectors are listed in Table 2.2, along with qualitative ratings (by number of gammas rather than stars) of their absorption, resistivity, charge transport and crystal quality.

Silicon and germanium have been widely developed in the semiconductor device industry. High-quality crystals with low trapping are readily available, but neither material has the gamma-ray absorption that would be desired at higher gamma-ray energies. Silicon is restricted to 30 keV or below, while thick germanium detectors are marginally useful at 140 keV. However, germanium is expensive and requires complex cryogenics, typically operating at around 100 K.

Mercuric iodide and thallium bromide have excellent gamma-ray absorption and high resistivity, but unfortunately the resistivity is obtained in part by low mobility. Crystal quality is still lacking, and HgI₂ is soft and difficult to work with.

Cadmium telluride and cadmium zinc telluride appear to be the best compromise at this writing, rating 2–3 gammas in each key characteristic.

Table 2.2. Comparison of some common semiconductor materials.

	Gamma-ray absorption	Resistivity	Charge Transport	Crystal quality
Si	γ	$\gamma\gamma$	$\gamma\gamma\gamma\gamma\gamma$	$\gamma\gamma\gamma\gamma\gamma$
Ge	$\gamma\gamma$	γ	$\gamma\gamma\gamma\gamma\gamma$	$\gamma\gamma\gamma\gamma\gamma$
CdTe	$\gamma\gamma\gamma$	$\gamma\gamma$	$\gamma\gamma\gamma$	$\gamma\gamma\gamma$
CZT	$\gamma\gamma\gamma$	$\gamma\gamma\gamma$	$\gamma\gamma\gamma$	$\gamma\gamma$
HgI ₂	$\gamma\gamma\gamma\gamma$	$\gamma\gamma\gamma\gamma\gamma$	$\gamma\gamma$	$\gamma\gamma$
TlBr	$\gamma\gamma\gamma\gamma$	$\gamma\gamma\gamma\gamma$	γ	$\gamma\gamma$

5.3.3 Typical length scales. In Section 4.1.2, we examined the size of the region of energy deposition for a 140 keV gamma ray interacting in CZT; in Section 5.2.4, we presented some considerations on pixel size. To see how these pieces fit together and what they imply for small-animal SPECT with semiconductor detectors, we now summarize the typical length scales for a CZT detector operating at 1000 V/cm bias and used with 140 keV gamma rays. The relevant lengths are given approximately by:

Attenuation length:	2.5 mm
Detector thickness:	1-2 mm
Range of photoelectron:	20
Range of K x ray:	100 μm
Pixel pitch (Arizona Hybrid):	380 μm
Feasible pixel pitch:	50-100 μm
Diameter of “diffusion ball”:	100 μm
Electron drift length:	2 cm
Hole drift length:	200 μm

As noted, the effect of the small hole drift length can be mitigated by using small pixels, although then the charge sharing due to the range of the K x ray and carrier diffusion can become appreciable. However, neither of these effects should be regarded as a fundamental limit on resolution. As we shall discuss in more detail in the next chapter, much finer resolution can be obtained with accurate statistical models and optimal position estimation.

6. Scintillation detectors

The use of scintillation detectors in gamma-ray imaging, and especially in small-animal SPECT, is surveyed in this section. The organization is similar to that of Section 5; topics include the physics of light production, materials considerations, optical detectors, and camera configurations.

6.1 Physics of light production

6.1.1 Scintillation processes. The interaction of ionizing radiation with a scintillator creates an inner shell vacancy and an excited primary electron. Subsequently, a cascade of excited electrons is generated by radiative decay, auger processes, and inelastic electron-electron scattering. However, much of the energy dissipates as thermal energy, and the efficiency for generating ionized electrons can be quite low (15–50%). When the electron energies decrease below the ionization threshold, further nonradiative processes (thermalization, lattice relaxation, and charge trapping) can result, lowering the scintillation efficiency yet further. Processes resulting in the production of light can be divided into four categories:

Self-trapped, excitonic, and recombination luminescence. Unbound electrons and holes or bound e-h pairs (excitons) move mostly unperturbed in a perfect crystal, and spontaneous recombination is relatively slow. However, the probability for recombination is enhanced through localization of one or both charge carriers (trapping) as a result of lattice discontinuities or by a shared charge affinity of a group of atoms (self-trapping). Lattice discontinuities may be a result of atomic impurities, boundary conditions, or lattice defects that formed during crystallization. Furthermore, single charge carriers that have been trapped serve as Coulomb defects that can trap charge carriers of the opposite charge. Examples of materials that exhibit these scintillation processes are BaF_2 and pure NaI .

Intrinsic ion-activated luminescence. For some materials, an intrinsic ionic component of the crystal can luminesce by undergoing an intra-ionic transition or by a charge-transfer transition. Such ions are termed activation ions or luminescent species. Examples of such ions are Bi^{2+} in $\text{Bi}_4\text{Ge}_3\text{O}_{12}$ (BGO) and $[\text{WO}_4]^{2-}$ in CdWO_4 , respectively.

Dopant ion-activated luminescence. Some materials can be doped with impurity ions that serve to activate luminescence (see intrinsic ion-activation above). If the dopant activation ions are sparse, electron-hole pairs may be trapped and recombined by relatively few activation ions. This process could be inhibitive, slowing the scintillation response. However, the dopant-induced lattice defect results in an increased rate of electron-hole trapping. Examples of scintillators with dopant activators are $\text{LaBr}_3\text{:Ce}$, CsI:Na , and $\text{Lu}_2\text{SiO}_5\text{:Ce}$ (LSO).

Cross-luminescence or core-valence luminescence (CVL). When a vacancy forms in the top core band of a crystal, a valence electron transitions to fill the vacancy [Rodnyi, 1992]. If the energy generated in this process is less than the fundamental bandgap, then the process is Auger free, and CVL may occur. Although this de-excitation process is fast (~ 1 ns), initial ionization of core electrons is an inefficient process, yielding at most a few photons per keV. Examples of CVL scintillation occur in BaF_2 , CsCl , RbF , and BaLu_2F_8 .

6.1.2 Nonproportionality. The amount of light produced by a scintillator depends on the likelihood of the radiative and nonradiative processes dissipating the deposited energy. These likelihoods will depend on the conditions in the scintillator, including the scintillator composition, structure, temperature, and even the amount of deposited energy. Generally, we would like process likelihoods to be independent of the deposited energy and for the light production to be a constant gain process. However, the deposited energy often does affect conditions in the scintillator, resulting in nonlinearities in the response. Nonlinear deviations of the scintillator response are termed nonproportionality. Much work has been done to better understand and measure nonproportionality, see Dorenbos et al. [1995], and Moses [2002].

6.2 Materials

Scintillators commonly used in SPECT include thallium-doped NaI (NaI:Tl) and either thallium- or sodium-doped CsI. However, over the past several decades, there has been an intense search for brighter, faster, more reliable, and cost-effective alternatives; see Derenzo and Moses [1993], van Eijk [2002], and Weber [2002]. This research has resulted in a wealth of new scintillators and a significant advancement in performance and fundamental knowledge of scintillation processes.

Table 2.3 gives a list of many viable scintillators for use in small-animal SPECT. A more complete compilation with detailed references is posted on the CGRI webpage: <http://www.gamma.radiology.arizona.edu>.

Interestingly, NaI:Tl , which was developed a few years after the photomultiplier was invented (mid-1940s), remains a viable contender for use in SPECT. In addition to new scintillators, many new fabrication methods have been developed, including columnar growth of CsI:Tl (parallel columns grown by vapor deposition with length ~ 1 mm and diameter ~ 3 μm).

Criteria for material selection for small-animal SPECT include absorption lengths, light yield, decay times, energy resolution, mechanical and radiological durability, chemical stability, and price. Light yield is especially important for Anger-type scintillation cameras where the interaction position is to be estimated from the relative signal on different photodetectors; low light yield means poor signal-to-noise ratio and hence poor spatial resolution in such devices. Light yield also is important in energy resolution and hence scatter rejection, but this factor is less critical for small-animal imaging, where there is significantly less scatter from the object than in clinical imaging.

Table 2.3. Properties of some useful scintillation materials.

	Hygro- scopic	Max.Emis. Wavelng. (nm)	30KeV Att.Coeff (cm ⁻¹)	140KeV Att.Coeff (cm ⁻¹)	Decay Times (ns)	Light Yield (ph/KeV)
CeCl ₃	Yes	360	28.89	2.89	4.4(6%), 23(70%), 70(8%), >10000(16%)	28
Cs ₂ LiYCl ₆ :Ce	Yes	380	29.48	2.02	2(3%), 6500(97%)	22
CsI:Na	Yes	420	40.76	4.46	460(90%), 4180(10%)	39
CsI:Tl	Slightly	540	41.58	4.53	680(63%), 3340(37%)	65
Gd ₂ O ₂ S:Tb (GOS)	No	547	91.62	9.30	>4000	78
Gd ₃ Ga ₅ O ₁₂ :Cr,Ce	No	730	49.65	5.16	140000	40
K ₂ LaI ₅ :Ce	Yes	409	36.68	3.94	65(90%)	52
LaBr ₃ :Ce	Yes	358	79.09	3.42	35 (90%),	61
LaCl ₃ :Ce	Yes	350	27.93	2.82	20(70%), 213(30%)	49
Lu _{1.8} Y _{0.2} SiO ₅ :Ce (LYSO)	No	430	52.75	4.08	48	32-34
Lu ₂ O ₃ :Eu,Tb	No	611	167.37	16.28	>10,000	20
Lu ₂ S ₃ :Ce	No	592	101.91	9.78	32	28
Lu ₂ Si ₂ O ₇ :Ce (LPS)	No	385	86.55	8.51	38	26
Lu ₂ SiO ₅ :Ce (LSO)	No	430	115.41	11.28	47	27
LuI ₃ :Ce	Yes	465	68.50	7.07	34(79%), 630(21%)	47
NaI:Tl	Yes	415	28.19	3.12	230	38
RbGd ₂ Br ₇ :Ce	Yes	420	80.44	3.60	45(53%), 400(47%)	56
Y _{1.34} Gd _{0.60} O ₃ :(Eu,Pr) _{0.06} (YGO)	No	610	116.88	5.72	1000000	42
Y ₂ SiO ₅ :Ce (YSO)	No	420	39.74	0.95	70	45
YAlO ₃ :Ce (YAP)	No	350	71.71	1.81	25-31	20-21
ZnS:Ag	No	450	37.34	1.03	110	49

6.3 Segmented versus monolithic crystals

As mentioned in Section 3.2.4, scintillation crystals can be used as segmented or monolithic detectors. Many recently developed gamma imaging systems use arrays of segmented scintillation crystals coupled to position-sensitive optical detectors (e.g., MAPMT, APD, etc.). The multichannel outputs of the position-sensitive devices are then combined by using external resistive networks implementing Anger arithmetic into X and Y signals that are then used to identify the segment in which a gamma ray interacted; see Dhanasopon et al. [2003], Inadama et al. [2003] and Pani et al. [2003, 2004].

The advantage of this approach is that the final detector has a reasonable spatial resolution (essentially the size of the crystal segments, which have been as small as 1 mm²) in a compact, modular package. Disadvantages are that the crystal is fairly costly because of the segmentation, the sensitivity becomes smaller as the segment size is reduced (packing fraction decreases), the energy resolution is degraded because not all of the light gets out of the crystal segment, and there is no way to estimate depth of interaction (DOI) within the scintillator without auxiliary optical detectors or further segmentation.

In addition to lateral segmentation of the crystal, the crystal can be segmented to give DOI information. Segmentation in DOI is accomplished by encoding a change of the properties of the segments at different depths. This encoding can be done by

changing the scintillation properties (wavelength, pulse decay time, etc.) or even by changing the reflectivity of the septa between segments at different depths; see Orita et al. [2003] and Chung et al. [2003].

An alternative approach, under investigation at CGRI, is to use a monolithic (nonsegmented) scintillation crystal with a position-sensitive optical detector (e.g., Hamamatsu H8500 MAPMT). Instead of using Anger arithmetic as the first step, we propose to acquire all signal outputs for each event, either storing them individually for later processing or combining them on the fly into a smaller set of signals that preserve the pertinent information. A discussion of maximum-likelihood estimation methods for processing these data is given in Chapter 3.

6.4 Seeing the light

6.4.1 Photomultiplier tubes (PMTs). Since their conception in the mid-1940s, PMTs have been the workhorse in amplification of low-intensity optical signals. PMTs provide large gain, on the order of 10^6 or more, and amplification noise is typically small. For scintillation cameras, the most important PMT characteristics are the *spectral response* and the *quantum efficiency* (QE) of the photocathode.

The spectral response must be chosen to match the emission spectrum of the scintillator used. Because the most important scintillators emit in the blue or near UV, it is possible to use a photocathode with no response in the green or red. Such photocathodes have a large photoelectric work function and hence a large thermal work function; thus, dark current is almost nonexistent, even at room temperature.

As discussed in much more detail in the next chapter, the QE is critical in scintillation cameras because spatial and energy resolution are fundamentally limited by the Poisson statistics of the photoelectrons liberated at the photocathode. QE in the range of 15–50% is common, but for limited spectral ranges. For a bi-alkali photocathode (e.g., Sb-Rb-Cs, Sb-K-Cs), QE is about 20% in the visible range. Hydrogenated, polycrystalline diamond has a QE of about 35% in the UV range. For solid-state III-V photocathodes, such as GaAs(Cs) and GaAsP(Cs), a QE of nearly 50% for visible and 15% for near-infrared is possible.

6.4.2 Multi-anode PMTs. A number of groups have developed small gamma cameras based on position-sensitive photomultiplier tubes (PSPMTs). A PSPMT typically consists of four signal outputs at the corners of a resistive anode plane of a PMT (combinations of these outputs give the equivalent of the computed Anger signals of a modular Anger camera). Interest in this area has been boosted recently by the introduction of the flat-paneled multi-anode photomultiplier tube (MAPMT), which is essentially an array of PMTs in a single glass envelope.

Currently available devices such as the Hamamatsu H8500 now have 8×8 anodes in a $5 \text{ cm} \times 5 \text{ cm}$ area. Devices with even more anodes will soon be available. Keeping the same packaging size, Hamamatsu is in the final pre-production stages of a 16×16 anode device [Inadama, 2003], and Burle has a 32×32 MCP flip-chip device under development.

Electron multiplication in these flat-paneled devices is accomplished either by layers of dynode gratings (e.g., Hamamatsu H8500) or microchannel plates (Burle 85011). Due to their size and geometry, these devices have a large percent active area, minimal anode cross talk, and excellent pulse resolution. For example, the H8500 has 89% active area, <3% crosstalk, and 300psec pulse resolution [Hadig, 2002].

6.4.3 Photodiodes. Because silicon photodiodes are highly developed and have high quantum efficiency, it is natural to inquire into their usefulness as photodetectors in scintillation cameras. The main drawback of photodiodes is that they have no internal gain mechanism; thus, the noise associated with the detector and the external electronics will be much more serious than for PMTs.

The major noise components to be considered are the thermal noise of the photodiode, shot noise from leakage current through the diode, and thermal and 1/f noise in the amplifier that follows the photodiode and integrates the current to obtain a measure of the charge associated with each gamma-ray event. These different noise sources have different effects depending on the response characteristics of the amplifier and pulse-shaping network; for a detailed discussion, see Radeka [1988].

The analysis by Radeka shows that there are several terms in the variance of the noise charge, but the one of interest in this discussion is proportional to the mean-square amplifier noise multiplied by the square of the total capacitance seen at the amplifier input. The total capacitance includes the photodiode capacitance as well as that of the integrating capacitor and any cables used. Large-area photodiodes have large capacitance as well as large leakage current; therefore, in practice, the use of photodiodes with scintillators is limited to devices only a few millimeters across [Bird, 1993; Moses, 1994, 1995].

An interesting variant on simple planar photodiodes is the silicon drift detector [Gatti and Rehak, 1984]. These devices have small, point-like anodes so they can have large optical collection area but small capacitance.

Materials other than silicon also have been used for photodiodes in scintillation-counting applications. For example, HgI₂ photodiodes have been used with CsI(Tl) scintillators by Wang et al. [1995].

6.4.4 Avalanche photodiodes. Avalanche photodiodes (APDs) are silicon diodes operated at large reverse bias so that the carriers gain enough energy to excite new electron-hole pairs, in a manner similar to the gas proportional counters discussed in Section 4.3.3. Thus they function like PMTs, as photodetectors with internal gain. Because the gain can occur at any point in the depletion region, rather than at discrete dynodes as in PMTs, however, the gain noise tends to be larger in APDs.

It is also possible to construct APDs with resistive anodes in such a way as to obtain signals related to the position where a photon is absorbed. Hence, these so-called position-sensitive APDs function like miniature Anger cameras.

6.4.5 Video detectors. Because optical cameras have much better spatial resolution than gamma-ray cameras, it is natural to inquire whether it is possible to obtain high intrinsic resolution for gamma rays simply by imaging a scintillation crystal onto an optical camera. This idea has been evaluated by numerous groups in the past, but usually it has been rejected on statistical grounds. If the required field of view (size of the scintillation crystal) is $L \times L$ and the area of the optical camera is $w \times w$, with $w \ll L$, then the crystal must be demagnified by a factor of w/L , and the optical collection efficiency of the lens is reduced by the square of this quantity. As a result, the number of photoelectrons produced in one pixel of the optical camera for a single gamma-ray interaction may drop below one, or at least below the noise floor set by dark current and read noise. Under these conditions, the detective quantum efficiency of the system can be considerably less than the absorption efficiency of the scintillator. Moreover, even if an adequate number of photoelectrons per gamma ray can be produced, the system still operates as an integrating detector rather than a photon-counting one; therefore, energy discrimination is not possible, and the noise properties of the image suffer further, as discussed in Section 4.2.2.

Several developments over the last two years suggest that we should reconsider these conclusions. First, optical detector arrays are now much larger and have much lower noise than before; 6 cm \times 6 cm CCDs (charge-coupled devices) are now available at reasonable cost and, when cooled modestly, they have essentially no dark current. Noise in the readout electronics also is being reduced by built-in electron multiplication or parallel readout. Moreover, these new devices have very high quantum efficiency for incident optical photons, over 90% in some cases; for comparison, conventional PMTs have a quantum efficiency around 25–30%.

Most important, for application to small-animal imaging, the field of view can be much smaller, and it is even possible to use 1 : 1 magnification for imaging the scintillator onto the CCD. With this magnification and well-corrected lenses of large numerical aperture, the optical-photon collection efficiency can be excellent.

Another motivation for lens-coupled gamma cameras is the current strong interest in bioluminescence and fluorescence studies in small animals. Many laboratories already have a low-noise CCD camera, and it should be possible to add a scintillator and suitable optics to convert it into a dual-modality SPECT/optical imager.

7. Summary and future directions

Progress in small-animal SPECT requires better temporal and spatial resolution in the final images, and this in turn requires better detectors. Improvements can be measured broadly in terms of the usable space-bandwidth product of the detector system which, as discussed in Sec. 2.2.3, can be used to improve either the final image resolution, the system sensitivity, or both. It is also important that detectors to be used with pinholes be able to resolve the depth of interaction and, when multiple pinholes are used, the detectors must have high count-rate capability. Of the conventional detector characteristics, perhaps the least important in small-animal SPECT is energy resolution.

Although new technologies such as superconducting tunnel junctions and gas ionization devices may hold promise in the long run, significant improvements in detector performance are still possible with relatively conventional scintillation cameras and semiconductor detector arrays.

As with any engineering effort, performance of the final system is closely tied to characteristics of the materials used. For scintillation detectors, there is a continuing need for brighter, faster scintillation crystals; for semiconductor arrays, the need is for better charge transport and material homogeneity. In both cases, high density and high atomic number are very desirable.

Improved system performance can often be achieved by use of modular detectors, with each unit mechanically, optically, and electronically independent of all others. The modular approach allows flexibility in system design, high count-rate capability, and easy interchangeability for maintenance and design modification.

A less-obvious route to improved imaging systems is through the use of rigorous methods from statistical decision theory. The performance of all gamma-ray imaging systems is limited by the random fluctuations of the object, the Poisson statistics of the gamma-ray flux, and the signals produced by each photon; it is crucial to understand these limitations if one is to analyze and systematically optimize system performance. Specifically for gamma-ray detectors, it is important to catalog all of the noise sources that influence our ability to detect and localize individual gamma-ray events, to develop rigorous statistical characterizations of each noise source, and to use this statistical knowledge in optimal signal processing. These issues will be dealt with in the next chapter.

The future for small-animal SPECT is bright. As we noted in Section 3.2.3, the linear resolution of current small-animal PET and SPECT systems is about 1 mm isotropically, corresponding to a volume resolution of about 1 μL and making it reasonable to characterize the systems as microPET or microSPECT. It follows from the discussion of detector technologies presented in this chapter that a resolution of 100 μm is currently within reach for small-animal SPECT (although probably not for small-animal PET), and this linear resolution corresponds to a volume resolution of 1 nL. True NanoSPECT is probably achievable within two years of this publication. True picoSPECT (10 μm linear, 1 pL volumetric resolution) is not out of the question, at least for ^{125}I imaging.

References

- [Abbey, 1995] C. K. Abbey, H. H. Barrett, "Linear iterative reconstruction algorithms: Study of observer performance," *XIVth International Conference on Information Processing in Medical Imaging (IPMI)*, Ile de Berder, France, pp. 65-76, June 26-30, 1995.
- [Abbey, 1996] C. K. Abbey, H. H. Barrett, D. W. Wilson, "Observer signal-to-noise ratios for the ML-EM algorithm," *Proc SPIE*, vol. 2708, 1996.
- [Accorsi, 2001a] R. Accorsi, F. Gasparini, R. C. Lanza, "A Coded Aperture for High-Resolution Nuclear Medicine Planar Imaging with a Conventional Anger

- Camera: experimental results,” *IEEE Trans Nucl Sci*, vol. 48, no. 6, pp. 2411-2417, December 2001a.
- [Accorsi, 2001b] R. Accorsi, F. Gasparini, R. C. Lanza, “Optimal Coded Patterns for Improved SNR in Nuclear Medicine Imaging,” *Nucl Instr Meth Phys Res A*, vol. 474, pp. 273-284, 2001b.
- [Barrett, 1972] H. H. Barrett, “Fresnel zone plate imaging in nuclear medicine,” *J. Nucl Med*, vol. 13, no. 6, pp. 382-385, 1972.
- [Barrett, 1981] H. H. Barrett, W. Swindell, *Radiological Imaging: Theory of Image Formation, Detection, and Processing*, vols. I and II, New York, Academic Press, 1981.
- [Barrett, 1990] H. H. Barrett, “Objective assessment of image quality: effects of quantum noise and object variability,” *J. Opt Soc Am A*, vol. 7, pp. 1266-1278, 1990.
- [Barrett, 1994] H. H. Barrett, H. C. Gifford, “Cone-beam tomography with discrete data sets,” *Phys Med Biol*, vol. 39, pp. 451-476, 1994.
- [Barrett, 1995a] H. H. Barrett, J. L. Denny, R. F. Wagner, K. J. Myers, “Objective assessment of image quality. II Fisher information, Fourier crosstalk, and figures of merit for task performance,” *J. Opt Soc Am A*, vol. 12, no. 5, pp. 834-852, 1995a.
- [Barrett, 1995b] H. H. Barrett, J. D. Eskin, H. B. Barber, “Charge transport in arrays of semiconductor gamma-ray detectors,” *Phys Rev Lett*, vol. 75, no. 1, pp. 156-159, 1995b.
- [Barrett, 1996a] H. H. Barrett, J. L. Denny, H. C. Gifford, C. K. Abbey, “Generalized NEQ: Fourier analysis where you would least expect to find it,” *Proc SPIE*, vol. 2708, pp. 41-52, 1996a.
- [Barrett, 1996b] H. H. Barrett, W. Swindell, *Radiological Imaging: Theory of Image Formation, Detection, and Processing*, Paperback edition, New York, Academic Press, 1996b.
- [Barrett, 1998] H. H. Barrett, B. Gallas, E. Clarkson, A. Clough, “Scattered radiation in nuclear medicine: A case study in the Boltzmann transport equation,” *Computational Radiology and Imaging: Therapy and Diagnosis*, Borgers, C., Natterer, F. eds., Springer Verlag, 1998.
- [Barrett, 2004] H. H. Barrett, K. J. Myers, *Foundations of Image Science*, New York, John Wiley and Sons, 2004.
- [Bird, 1993] A. J. Bird, T. Carter, A. J. Dean, D. Ramsden, B. M. Swinyard, “The optimisation of small CsI(Tl) gamma-ray detectors,” *IEEE Trans Nucl Sci*, vol. 40, no. 4, pp. 395-399, 1993.
- [Breskin, 2002] A. Breskin, A. Buzulutskov, R. Chechik, B. K. Singh, A. Bondar, L. Shekhtman, “Sealed GEM photomultiplier with a CsI photocathode,” *Nucl Instr Meth Phys Res A*, vol. 478, pp. 225-229, 2002.
- [Chen, 1997] J. C. Chen, “Scatter Rejection in Gamma Cameras for Use in Nuclear Medicine,” *Biomed Eng Appl Basis Comm*, vol. 9, pp. 20-26, 1997.

- [Chung, 2003] Y. H. Chung, Y. Choi, G. Cho, Y. S. Choe, K.-H. Lee, B.-T. Kim, "Optimization of Dual Layer Phoswich Detector Consisting of LSO and LuYAP for Small Animal PET," *Proc IEEE Med Imag Conf*, 2003.
- [Clarkson, 1999] E. Clarkson, D. W. Wilson, H. H. Barrett, "The synthetic collimator for 2D and 3D imaging," *Proc SPIE Med Imag*, vol. 3659, pp. 107-117, 1999.
- [Derenzo, 1993] S. E. Derenzo, W. W. Moses, "Experimental efforts and results in finding new heavy scintillators," *Heavy Scint for Sci and Indust Apps*, De Notaristefani, F., LeCoq, P., Schneegans, M. eds., Gif-sur-Yvette, France, Editions Frontieres, pp. 125-135, 1993.
- [Dhanasopon, 2003] A. P. Dhanasopon, C. S. Levin, A. M. K. Foudray, P. D. Olcott, J. A. Talcott, F. Habte, "Scintillation Crystal Design Features for a Miniature Gamma Ray Camera," *Proc IEEE Med Imag Conf*, 2003.
- [Dorenbos, 1995] P. Dorenbos, J. T. M. de Haas, C. W. E. van Eijk, "Non-proportionality in Scintillator Response and Energy Resolution Obtainable with Scintillator Crystals," *IEEE Trans Nucl Sci*, vol. 42, pp. 2190-2202, 1995.
- [Eskin, 1999] J. D. Eskin, H. H. Barrett, H. B. Barber, "Signals induced in semiconductor gamma-ray imaging detectors," *J. Appl Phys*, vol. 85, pp. 647-659, 1999.
- [Furenlid, 2000] L. R. Furenlid, E. Clarkson, D. G. Marks, H. H. Barrett, "Spatial pileup considerations for pixellated gamma-ray detectors," *IEEE Trans Nucl Sci*, vol. 47, pp. 1399-1402, 2000.
- [Gatti, 1984] E. Gatti, P. Rehak, "Semiconductor drift chamber – an application of a novel charge transport scheme," *Nucl Instr Meth*, vol. 225, pp. 608-614, 1984.
- [Gunter, 1996] D. L. Gunter, "Collimator Characteristics and Design." In *Nuclear Medicine*, Henken, R. E., ed., Mosby Year Book, St. Louis, Chap. 8., 1996.
- [Hadig, 2002] T. Hadig, J. Schwiening, C. Field, G. Mazaheri, M. Jain, D. G. W. S. Leith, B. Ratcliff, J. Va'vra, "Study of Timing and Efficiency Properties of the Hamamatsu H-8500 Photomultiplier," *Proc IEEE Nucl Sci Symp*, 2002.
- [Inadama, 2003] N. Inadama, H. Murayama, M. Watanabe, T. Omura, T. Yamashita, H. Kawai, N. Orita, T. Tsuda, "Performance of 256ch flat panel PS-PMT with small crystals for a DOI PET detector," *Proc IEEE Med Imag Conf*, 2003.
- [Jaszczak, 1994] R. J. Jaszczak, J. Li, H. Wang, M. R. Zalutsky, R. E. Coleman, "Pinhole collimation for ultra-high resolution, small-field-of-view SPECT studies," *Phys Med Biol*, vol. 39, pp. 425-437, 1994.
- [Knoll, 1999] G. F. Knoll, *Radiation Detection and Measurement*, 3rd ed., New York, Wiley, 1999.
- [Kwo, 1991] D. P. Kwo, H. B. Barber, H. H. Barrett, T. S. Hickernell, J. M. Woolfenden, "Comparison of NaI(Tl), HgI₂ and CdTe surgical probes II: Effect of scatter compensation on probe performance," *Med Phys*, vol. 18, pp. 382-389, 1991.

- [Marks, 1999] D. G. Marks, H. B. Barber, H. H. Barrett, J. Tueller, J. M. Woolfenden, "Improving performance of a CdZnTe imaging array by mapping the detector with gamma rays," *Nucl Instr Meth Phys Res A*, vol. 428, pp. 102-112, 1999.
- [Matteson, 1997] J. L. Matteson, W. Coburn, F. Duttweiler, W. A. Heindl, G. L. Huszar, P. C. LeBlanc, M. R. Pelling, L. E. Peterson, R. E. Rothschild, R. T. Skelton, P. L. Hink, C. Crabtree, "CdZnTe arrays for astrophysics applications," *Proc SPIE*, vol. 3115, pp. 160-175, 1997.
- [McCready, 1971] V. R. McCready, R. P. Parker, E. M. Gunnensen, R. Ellis, E. Moss, W. G. Gore, "Clinical tests with a prototype semiconductor gamma camera," *Brit J. Radiology*, vol. 44, pp. 58, 1971.
- [Meikle, 2003a] S. R. Meikle, R. Wojcik, A. G. Weisenberger, M. F. Smith, S. Majewski, P. Kench, S. Eberl, R. R. Fulton, M. Lerch, A. B. Rosenfeld, "CoALA-SPECT: A coded aperture laboratory animal SPECT system for preclinical imaging," *2002 IEEE Nucl Sci Symp Conference Record*, Scott Metzler, ed., Norfolk, Virginia, ISBN 0-7803-7637-4, November 10-16, 2002a.
- [Meikle, 2003b] S. R. Meikle, P. Kench, A. G. Weisenberger, R. Wojcik, M. F. Smith, S. Majewski, S. Eberl, R. R. Fulton, A. B. Rosenfeld, M. J. Fulham, "A prototype coded aperture detector for small animal SPECT," *IEEE Trans Nucl Sci*, vol. 49, pp. 2167-2171, 2003b.
- [Mörmann, 2002] D. Mörmann, A. Breskin, R. Chechik, P. Cwetanski, B. K. Singh, "Gas avalanche photomultiplier with a CsI-coated GEM," *Nucl Instr Meth Phys Res A*, vol. 478, pp. 230-234, 2002.
- [Moses, 1994] W. W. Moses, S. E. Derenzo, "Design studies for a PET detector module using a pin photodiode to measure depth of interaction," *IEEE Trans Nucl Sci*, vol. 41, no. 4, pp. 1441-1445, August 1994.
- [Moses, 1995] W. W. Moses, S. E. Derenzo, C. L. Melcher, R. A. Manente, "A room temperature LSO/pin photodiode PET detector module that measures depth of interaction," *IEEE Trans Nucl Sci*, vol. 42, no. 4, pp. 1085-1089, August 1995.
- [Moses, 2002] W. W. Moses, "Current trends in scintillator detectors and materials," *Nucl Instr Meth Phys Res A*, vol. 487, pp. 123-128, 2002.
- [Muehllehner, 1985] G. Muehllehner, "Effect of resolution improvement on required count density in ECT imaging: a computer simulation," *Phys Med Biol*, vol. 30, no. 2, pp. 163-173, 1985.
- [Müller, 1986] S. P. Müller, J. F. Polak, M. F. Kijewski, B. L. Holman, "Collimator Selection for SPECT Brain Imaging: The Advantage of High Resolution," *J. Nucl Med*, vol. 27, pp. 1729-1738, 1986.
- [Myers, 1990] K. J. Myers, J. P. Rolland, H. H. Barrett, R. F. Wagner, "Aperture optimization for emission imaging: Effect of a spatially varying background," *J. Opt Soc Am A*, vol. 7, pp. 1279-1293, 1990.

- [Orita, 2003] N. Orita, H. Murayama, H. Kawai, N. Inadama, T. Tsuda, "Three Dimensional Array of Scintillation Crystals with Proper Reflector Arrangement for a DOI detector," *Proc IEEE Med Imag Conf*, 2003.
- [Pani, 2003] R. Pani, R. Pellegrini, M. N. Cinti, C. Trotta, G. Trotta, R. Scafe, M. Betti, F. Cusanno, L. Montani, G. Iurlaro, F. Garibaldi, Del A. Guerra, "A novel compact gamma camera based on flat panel PMT," *Nucl Instr Meth Phys Res A*, vol. 513, no. 1, pp. 36-41, 2003.
- [Pani, 2004] R. Pani, R. Pellegrini, M. N. Cinti, M. Mattioli, C. Trotta, L. Montani, G. Iurlaro, G. Trotta, D'L. Addio, S. Ridolfi, De G. Vincentis, I. N. Weinberg, "Recent advances and future perspectives of position sensitive PMT," *Nucl Instr Meth Phys Res B*, vol. 213, pp. 197-205, 2004.
- [Radeka, 1988] V. Radeka, "Low-noise techniques in detectors," *Ann Rev Nucl Part Sci*, vol. 38, pp. 217-277, 1988.
- [Rodnyi, 1992] P. A. Rodnyi, "Core-valence band transitions in wide-gap ionic crystals," *Sov Phys Solid State*, vol. 34, pp. 1053-1066, 1992
- [Rogulski, 1993] M. M. Rogulski, H. B. Barber, H. H. Barrett, R. L. Shoemaker, J. M. Woolfenden, "Ultra-high-resolution brain SPECT: simulation results," *IEEE Trans Nucl Sci*, vol. 40, pp. 1123-1129, 1993.
- [Rolland, 1989] J. P. Rolland, H. H. Barrett, G. W. Seeley, "Quantitative study of deconvolution and display mappings for long-tailed point-spread functions," *Proc SPIE*, vol. 1092, pp. 17-21, 1989.
- [Rolland, 1990] J. P. Rolland, *Factors influencing lesion detection in medical imaging*, Ph.D. Dissertation, University of Arizona, Tucson, Arizona, 1990.
- [Rolland, 1991] J. P. Rolland, H. H. Barrett, G. W. Seeley, "Ideal versus human observer for long-tailed point spread functions: Does deconvolution help?" *Phys Med Biol*, vol. 36, no. 8, pp. 1091-1109, 1991.
- [Rolland, 1992] J. P. Rolland, H. H. Barrett, "Effect of random background inhomogeneity on observer detection performance," *J. Opt Soc Am A*, vol. 9, no. 5, pp. 649-658, 1992.
- [Ryan, 1995] J. M. Ryan, J. R. Macri, M. L. McConnell, B. K. Dann, M. L. Cherry, T. G. Guzik, F. P. Doty, B. A. Apotovsky, J. F. Butler, "Large area sub-millimeter resolution CdZnTe strip detector for astronomy," *Proc SPIE*, vol. 301, pp. 2518:292, 1995.
- [Schramm, 2002] N. Schramm, G. Ebel, U. Engeland, M. Behe, T. Schurrat, T. M. Behr, "Multi-pinhole SPECT for small animal research," *J. Nucl Med*, vol. 43, no. 5, pp. S.913, 2002.
- [Smith, 1998] M. F. Smith, R. Jaszczak, "An analytic model of pinhole aperture penetration for 3D pinhole SPECT image reconstruction," *Phys Med Biol*, vol. 43, pp. 761-775, 1998.
- [Stahle, 1996] C. M. Stahle, A. Parsons, L. M. Bartlett, P. Kurczynski, J. F. Krizmanic, L. M. Barbier, S. D. Barthelmy, F. Birsas, N. Gehrels, J. Odom, D. Palmer, C. Sappington, P. Shu, Teegarden B. J., J. Tueller, "CdZnTe strip detector for

- arc second imaging and spectroscopy,” *Proc Society Photo-Optical and Instr Eng*, vol. 2859, pp. 74-84, 1996.
- [Tsui, 1978] B. M. W. Tsui, C. E. Metz, F. B. Atkins, S. J. Starr, R. N. Beck, “A Comparison of Optimum Detector Spatial Resolution in Nuclear Imaging based on Statistical Theory and on Observer Performance,” *Phys Med Biol*, vol. 23, no. 4, pp. 654-676, 1978.
- [Tsui, 1983] B. M. W. Tsui, C. E. Metz, Beck, R. N. “Optimum detector spatial resolution for discriminating between tumour uptake distributions scintigraphy,” *Phys Med Biol*, vol. 28, no. 7, pp. 775-788, 1983.
- [Wagner, 1985] R. F. Wagner, D. G. Brown, “Unified SNR analysis of medical imaging systems,” *Phys Med Biol*, vol. 30, no. 6, pp. 489-518, 1985.
- [Wang, 1995] Y. J. Wang, B. E. Patt, J. S. Iwanczyk, S. R. Cherry, Y. Shao, “High efficiency CsI(Tl)/HgI₂ 2 gamma ray spectrometers,” *IEEE Trans Nucl Sci*, vol. 42, no. 4, pp. 601-605, 1995.
- [White, 1994] T. A. White, *SPECT reconstruction directly from photomultiplier tube signals*, Ph.D. Dissertation, University of Arizona, Tucson, Arizona, 1994.
- [Weber, 2002] M. J. Weber, “Inorganic scintillators: today and tomorrow,” *J. Lums*, vol. 100, pp. 35-45, 2002.
- [Wilson, 2000] D. W. Wilson, E. W. Clarkson, H. H. Barrett, “Reconstruction of two- and three-dimensional images from synthetic collimator data,” *IEEE Trans Med Im*, vol. 19, no. 5, pp. 412-422, 2000.
- [van Eijk, 2002] van C. W. E. Eijk, “Inorganic scintillators in medical imaging,” *Phys Med Biol*, vol. 47, pp. R85-R106, April 21, 2002

Small-Animal SPECT Imaging

Kupinski, M.A.; Barrett, H.H. (Eds.)

2005, XXII, 294 p. 123 illus., Hardcover

ISBN: 978-0-387-25143-1